

ORIGINAL RESEARCH

Open Access



Comparison of standardized uptake values between ^{99m}Tc -HDP SPECT/CT and ^{18}F -NaF PET/CT in bone metastases of breast and prostate cancer

Samuli Arvola^{1*}, Ivan Jambor², Anna Kuisma³, Jukka Kempainen⁴, Sami Kajander⁴, Marko Seppänen^{1,4} and Tommi Nojonen^{1,5}

Abstract

Background: Despite recent technological advances allowing for quantitative single-photon emission computed tomography (SPECT), quantitative SPECT has not been widely used in the clinical practice. The aim of this study is to evaluate the feasibility of quantitative SPECT for measuring metastatic bone uptake in breast and prostate cancer by comparing standard uptake values (SUVs) measured with ^{99m}Tc -HDP SPECT/CT and ^{18}F -NaF PET/CT.

Methods: Twenty-six breast and 27 prostate cancer patients at high risk of bone metastases underwent both ^{99m}Tc -HDP SPECT/CT and ^{18}F -NaF PET/CT within 14 days of each other. The SPECT and PET data were reconstructed using ordered-subset expectation-maximization algorithms achieving quantitative images. Metastatic and benign skeletal lesions visible in both data sets were identified, and their maximum, peak, and mean SUVs (SUV_{max} , SUV_{peak} , and SUV_{mean}) were determined. SUV ratios (SUVRs) between the lesions and adjacent normal appearing bone were also calculated. Linear regression was used to evaluate the correlations between the SUVs of SPECT and PET and Bland-Altman plots to evaluate the differences between the SUVs and SUVRs of SPECT and PET.

Results: A total of 231 skeletal lesions, 129 metastatic and 102 benign, were analyzed. All three SUV measures correlated very strongly between SPECT and PET ($R^2 \geq 0.80$, $p < 0.001$) when all lesions were included, and the PET SUVs were significantly higher than SPECT SUVs ($p < 0.001$). The median differences were 21%, 12%, and 19% for SUV_{max} , SUV_{peak} , and SUV_{mean} , respectively. On the other hand, the SUVRs were similar between SPECT and PET with median differences of 2%, -9%, and 2% for SUVR_{max} , $\text{SUVR}_{\text{peak}}$, and $\text{SUVR}_{\text{mean}}$, respectively.

Conclusion: The strong correlation between SUVs and similar SUVRs of ^{99m}Tc -HDP SPECT/CT and ^{18}F -NaF PET/CT demonstrate that SPECT is an applicable tool for clinical quantification of bone metabolism in osseous metastases in breast and prostate cancer patients.

Keywords: Quantitative SPECT, SUV SPECT, SUV comparison, SUV ratio, Bone metastases

* Correspondence: samuli.arvola@tyks.fi

¹Department of Clinical Physiology and Nuclear Medicine, Turku University Hospital, Kiinamyllynkatu 4-8, 20521 Turku, Finland
Full list of author information is available at the end of the article

Background

Single-photon emission computed tomography (SPECT) has conventionally been used in a non-quantitative manner, i.e., the images have been interpreted using relative intensity values instead of absolute values of tracer concentration [1, 2]. However, the wide acceptance of integrated SPECT/CT scanners and the development of iterative reconstruction algorithms have made the clinical use of quantitative SPECT possible [3, 4]. Several applications for quantitative SPECT have been suggested but they have not been widely adopted in clinical routine use yet [1].

SPECT/CT with ^{99m}Tc -labeled diphosphonates, such as ^{99m}Tc -hydroxyethylene diphosphonate (HDP), is increasingly used for the detection of bone metastases in breast and prostate cancer patients [5]. The sensitivity and specificity of SPECT/CT are superior compared to conventional bone scintigraphy or SPECT alone [6, 7]. ^{18}F -NaF PET/CT is an even more sensitive method than ^{99m}Tc -diphosphonate SPECT/CT [6, 8], and PET is inherently quantitative [9]. However, ^{18}F -NaF PET/CT is rather expensive and has limited availability [2, 6].

Quantitative SPECT and PET allow the calculation of standardized uptake values (SUVs), which can be utilized for longitudinal disease assessment and interpatient comparison [10]. Feasibility of quantitative bone SPECT has been previously demonstrated by reporting skeletal SUVs [2, 11–14]; however, a direct comparison to a standard reference method, such as PET/CT, has not yet been performed. ^{18}F -NaF PET/CT has been validated using bone biopsy findings [15, 16] and proven to be repeatable in patients with bone metastases [17, 18], therefore being a potential standard method for the diagnosis of metastatic bone disease.

In this study, our aim is to explore the correlation between SUVs measured by quantitative ^{99m}Tc -HDP SPECT/CT and those measured by ^{18}F -NaF PET/CT in the evaluation of metastatic bone uptake in breast and prostate cancer patients.

Methods

Study design and patients

This study included the same patients as a previously published study by Jambor et al. (NCT01339780, ClinicalTrials.gov) [6]. Twenty-six breast and 27 prostate cancer patients at high risk for bone metastases were prospectively enrolled between February 2011 and March 2013. Each patient gave written informed consent, and the study was approved by the local ethics committee. Patients were included if they had localized pain in the skeletal area suggesting bone metastases, suspicious laboratory findings (elevated alkaline phosphates, elevated PSA, or high PSA doubling time after prostatectomy), or suspicious histopathologic findings (stage N3a or higher in breast cancer patients, stage T3a or higher, and/or Gleason score of 4 + 3 or higher in prostate cancer patients). All patients underwent

^{99m}Tc -HDP SPECT/CT, ^{18}F -NaF PET/CT, and 1.5-T whole-body magnetic resonance imaging (MRI), including diffusion-weighted imaging (DWI), within 14 days in a varying order. The median (range) interval between ^{99m}Tc -HDP SPECT/CT and ^{18}F -NaF PET/CT was 3 (1–14) days [6].

^{99m}Tc -HDP SPECT/CT

The patients received intravenous injection of 672 ± 21 (mean \pm SD) MBq of ^{99m}Tc -HDP. The SPECT scans were performed 180 ± 24 (mean \pm SD) min after the injection using a Symbia T6, True Point SPECT/CT scanner (Siemens Healthcare, Erlangen, Germany) with the following parameters: low-energy high-resolution collimators, three bed positions, 180 projections over 360° with 9-s acquisition time per view, 128×128 matrix, 4.8×4.8 mm pixel size, and 4.8-mm slice thickness. Low-dose CT scans were acquired with 130 kV and 10 effective mAs. The CT data were reconstructed using a smooth attenuation-correction kernel B08s and a sharp bone kernel B65s.

The SPECT data were reconstructed with HybridRecon-Oncology SUV SPECT (version 1.3, HERMES Medical Solutions AB, Stockholm, Sweden) using the three-dimensional (3D) ordered-subset expectation-maximization (OSEM) algorithm with 10 iterations and 15 subsets [19]. A relatively high number of iterations was used to increase the spatial resolution of SPECT images closer to the spatial resolution of PET. The reconstruction included corrections for decay, attenuation, scatter, and collimator response. Attenuation correction was based on attenuation coefficient maps derived from the B08s CT images [20]. Scatter correction was performed with a Monte Carlo simulation using 10^5 simulated photons and two scatter update iterations [21]. The collimator response was corrected using a Gaussian diffusion model [22]. The images were postfiltered with a Gaussian filter of 7-mm full width at half maximum (FWHM).

SPECT scanner calibration

The SPECT scanner was calibrated by scanning a uniform Jaszczak phantom (Data Spectrum Corporation, Durham, NC, USA) without any inserts inside and filled with water and 150 MBq of ^{99m}Tc -pertechnetate. A conversion factor to convert the reconstructed counts into units of activity concentration (Bq/ml) was calculated as the ratio between true activity and reconstructed counts in a homogeneous volume of interest (VOI). The resulting conversion factor was 0.107 kBq/cps.

^{18}F -NaF PET/CT

The patients received intravenous injection of 209 ± 7 (mean \pm SD) MBq of ^{18}F -NaF. Whole-body PET scans were performed 64 ± 6 (mean \pm SD) min after the injection using a Discovery VCT PET/CT or Discovery PET/CT 690 scanner (GE Healthcare, Milwaukee, WI, USA). A static emission scan from feet to skull vertex was performed with 3- (VCT

scanner) or 2-min (690 scanner) acquisition time per bed position.

The PET data were corrected for decay, attenuation, scatter, random coincidences, and dead time. The data acquired with Discovery VCT PET/CT were reconstructed in a 128 × 128 matrix with a pixel size of 5.47 × 5.47 mm and slice thickness of 3.27 mm using VUE Point HD (GE Healthcare, Milwaukee, WI, USA), a fully 3D OSEM algorithm with 2 iterations and 28 subsets. Discovery PET/CT 690 data were reconstructed in a 192 × 192 matrix with a pixel size of 3.65 × 3.65 mm and a slice thickness of 3.27 mm using VUE Point FX-Sharp IR (GE Healthcare, Milwaukee, WI, USA), also a fully 3D OSEM algorithm with 2 iterations and 24 subsets incorporating time-of-flight and point-spread function information. The images acquired with Discovery VCT PET/CT and Discovery PET/CT 690 were postfiltered with Gaussian filters of 7- and 9-mm FWHM, respectively, to lower the spatial resolution of PET closer to the spatial resolution of SPECT.

The PET scanners were quarterly calibrated following the EANM/EARL FDG-PET/CT accreditation procedure [23].

Image analysis

Image analysis was performed using HybridViewer (version 2.6, HERMES Medical Solutions AB, Stockholm, Sweden), which converted values of activity concentration into SUVs according to the following equation:

$$SUV = \frac{\text{voxel activity concentration} \left(\frac{Bq}{ml} \right) \times \text{patient weight (g)}}{\text{decay corrected injected activity (Bq)}} \times 1 \frac{ml}{g} \tag{1}$$

Skeletal lesions visible in both SPECT and PET images were classified into benign and metastatic by the consensus of two experienced nuclear medicine physicians (Fig. 1). Localization CT images of PET/CT and SPECT/CT and anatomical and DWI MRI images were used to verify the lesion classification according to corresponding morphologic findings [6].

For analyzing purposes, the identified lesions were first segmented from PET images using a threshold of SUV > 15, which was lowered if the resulting VOI was clearly smaller than the area of increased uptake. Next, the same lesions were segmented from SPECT images using SUV thresholds that resulted in VOIs with the volumes similar to those in PET images.

Maximum, peak, and mean SUVs (SUV_{max}, SUV_{peak}, and SUV_{mean}) were calculated from the VOIs. SUV_{max} was determined as the SUV of the most active voxel within the VOI, SUV_{peak} as the average SUV of a 1-cm³ cube positioned within the lesion such that the enclosed average SUV was maximized, and SUV_{mean} as the average SUV of voxels in the specific VOI. The cubic VOI of

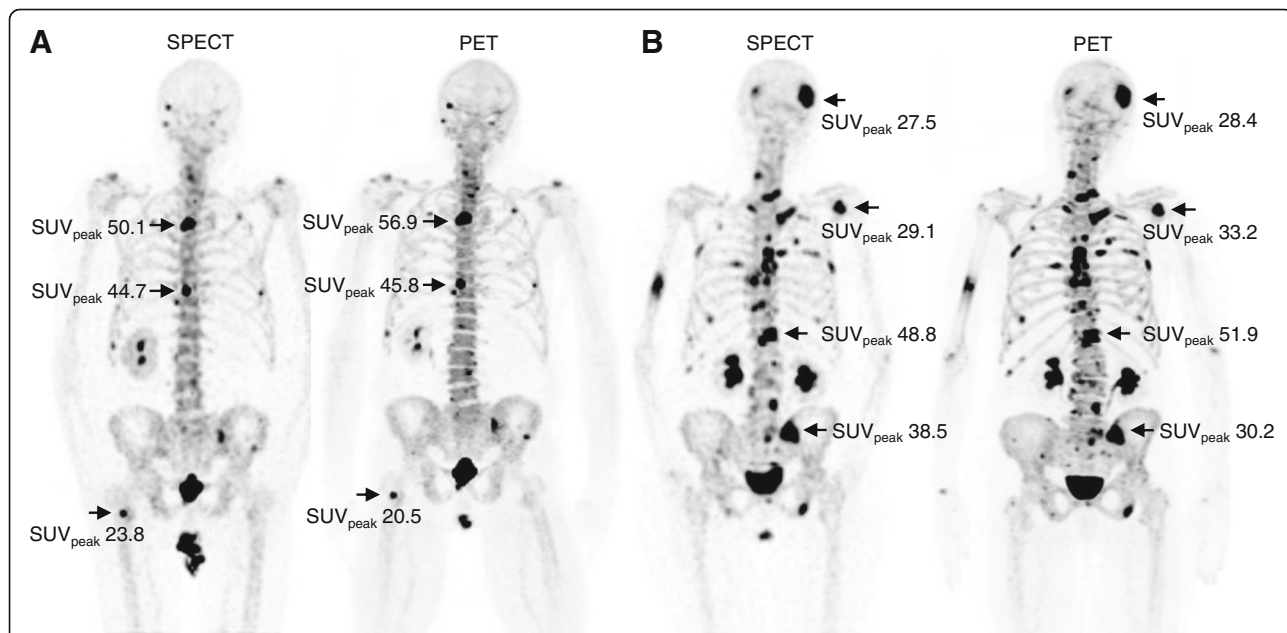


Fig. 1 Maximum intensity projections of ^{99m}Tc-HDP SPECT and ¹⁸F-NaF PET scans acquired (a) from the same 66-year-old prostate cancer patient and (b) from the same 75-year-old breast cancer patient. SUV_{peak} are shown for most active lesions. The SPECT scan of the prostate cancer patient was acquired 2 days before the corresponding PET scan and the SPECT scan of the breast cancer patient 5 days after the corresponding PET scan

SUV_{peak} could extend outside the lesion VOI in small lesions, which sometimes caused SUV_{peak} being lower than SUV_{mean} .

Background bone activity was determined separately for every lesion by placing five to ten circular regions of interest (ROIs) of 1-cm diameter on adjacent normal-appearing bone tissue. These ROIs were summed to form background VOI, whose mean SUV ($SUV_{mean,bg}$) was calculated. Maximum, peak, and mean SUV ratios ($SUVR_{max}$, $SUVR_{peak}$, and $SUVR_{mean}$) of the lesion were calculated by dividing the SUV_{max} , SUV_{peak} , and SUV_{mean} of the lesion by the corresponding $SUV_{mean,bg}$.

Statistical analyses

Statistical analyses were performed using MATLAB (version R2016A, The MathWorks, Natick, MA, USA) and SPSS (version 24, IBM Corp., Armonk, NY, USA) software. Scatter plots and linear regression models were used to evaluate the overall correlation between SUVs of SPECT and PET data, and the Bland-Altman plots were created to evaluate the agreement between SUVs and SUVRs of SPECT and PET data. In the Bland-Altman plots, the mean difference and 95% limits of agreement (LOA) were estimated using the median and the 2.5th and 97.5th percentiles of the differences because the differences were not normally distributed according to the Shapiro-Wilk test.

The Wilcoxon signed rank test was used to determine whether the SUVs and SUVRs of SPECT and PET were statistically different, and the Mann-Whitney U test was used to determine whether the SUVs and SUVRs of metastatic lesions were significantly higher than the SUVs and SUVRs of benign lesions. These nonparametric statistical methods were employed because the SUV and SUVR data were not normally distributed. Similarly, median and interquartile range (IQR or middle 50%) were used to report SUVs.

Results

A total of 231 skeletal lesions, 129 metastatic and 102 benign, were analyzed from 46 patients. The average SUV thresholds used for segmentation were 10.7 for SPECT and 12.9 for PET. Segmented lesion volumes varied from 0.55 to 60 cm³ with a median of 2.0 cm³, and the volumes were practically the same for the corresponding SPECT and PET lesions due to the segmentation method used (the volume difference ranged from 0 to 13% with a median of 2%). The number of analyzed lesions per patient varied from 0 to 21 with a median of 3. Metastatic lesions were analyzed from 18 patients and benign lesions from 37 patients. Seven patients had no identified lesions. Patient and lesion characteristics are listed in Table 1.

Scatter plots with regression lines for SUVs are shown in Fig. 2. Correlations between SPECT and PET SUVs are strong and statistically significant ($R^2 \geq 0.80$, $p < 0.001$), and PET SUVs are significantly higher than SPECT SUVs ($p < 0.001$). The regression lines have slopes close to one in all SUV analyses. y -intercepts suggest a constant bias between all SPECT and PET SUVs which is largest for SUV_{max} and smallest for SUV_{mean} (Fig. 2).

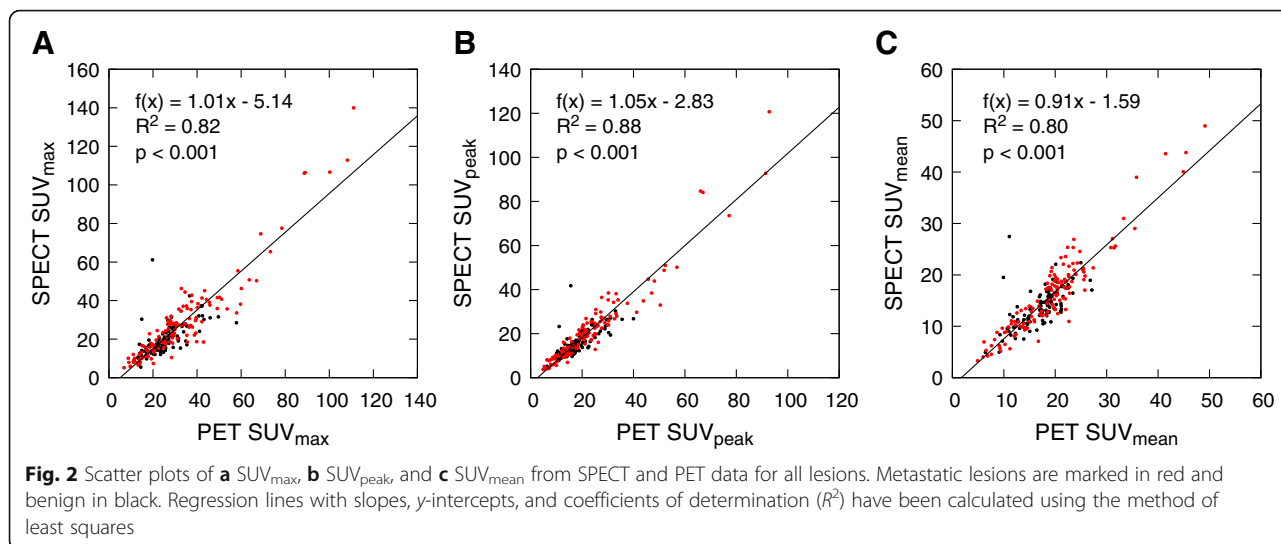
Metastatic lesions have generally higher SUVs than benign lesions, but the SUV distributions of benign and metastatic lesions overlap greatly (Fig. 2). According to the Mann-Whitney U test, the metastatic lesions had significantly higher PET SUV_{max} ($p < 0.05$), PET SUV_{peak} ($p < 0.01$), SPECT SUV_{peak} ($p < 0.01$), and SPECT SUV_{mean} ($p < 0.01$) than the benign lesions, but PET SUV_{mean} and SPECT SUV_{max} were not significantly different between benign and metastatic lesions. Therefore, SUV alone could not be used to differentiate metastatic and benign lesions.

The Bland-Altman plots of SUV_{max} , SUV_{peak} , and SUV_{mean} from SPECT and PET data are shown in Fig. 3. Among these analyses, SUV_{peak} reveals the smallest systematic difference and all SUV measures show only a moderate range of deviation and LOA for differences. The median differences (and LOA) normalized with respect to SPECT SUVs are 21% (−26–53%), 12% (−28–39%), and 19% (−11–45%) for SUV_{max} , SUV_{peak} , and SUV_{mean} , respectively. The effect of lesion volume on the SUV differences between SPECT and PET is shown in Table 2. The differences are smaller in larger lesions.

$SUV_{s,mean,bg}$ for different skeletal sites are listed in Table 3, and scatter plots with regression lines for SUVRs are shown in Fig. 4. Correlations between SPECT and PET SUVRs are slightly weaker than the

Table 1 Patient and lesion characteristics

	Breast cancer	Prostate cancer
Patients, n	26	27
Median age (range), years	61 (46–76)	67 (52–79)
Median height (range), cm	167 (158–175)	178 (169–186)
Median weight (range), kg	70 (56–99)	87 (60–110)
Metastatic lesions, n		
0	16	19
1–5	4	6
6–10	3	1
11–20	3	1
Benign lesions, n		
0	5	2
1–5	14	22
6–10	3	2
11–20	4	1



correlations between corresponding SUVs, but the regression lines are closer to the line of equality as their y-intercepts are almost 0. Even though the SUVR distributions of benign and metastatic lesions overlap like the SUV distributions, all SUVR measures are significantly different ($p < 0.001$) between benign and metastatic lesions.

The Bland-Altman plots for SUVR measures are shown in Fig. 5. SUVRs are even more similar than SUVs in Fig. 3 between SPECT and PET data because PET images have higher background SUVs than SPECT images (Table 3). According to the Wilcoxon signed rank test, only $SUVR_{peak}$ were statistically different between SPECT and PET data. The median differences (and LOA) normalized with respect to SPECT SUVs are 2% (-45–88%), -9% (-47–59%), and 2% (-42–65%) for $SUVR_{max}$, $SUVR_{peak}$, and $SUVR_{mean}$, respectively.

Discussion

We evaluated the correlation and similarity of SUVs and SUVRs between ^{99m}Tc -HDP SPECT and ^{18}F -NaF PET in different benign skeletal lesions and bone metastases of breast and prostate cancer patients. To our knowledge, this is the first study to report SUVs and SUVRs of ^{99m}Tc -diphosphonate SPECT using ^{18}F -NaF PET as a reference standard. Strong correlations were shown between SUVs and similarities between SUVRs of these two methods. Previous clinical research has mainly reported ^{99m}Tc -diphosphonate SPECT SUVs in different skeletal structures without direct reference values [2, 11–14]. Our results demonstrate that ^{99m}Tc -HDP SPECT SUVs and SUVRs reflect the metabolic activity of lesions similarly to ^{18}F -NaF PET SUVs and SUVRs; thus, SPECT measures can potentially be used to clinically evaluate bone metastases.

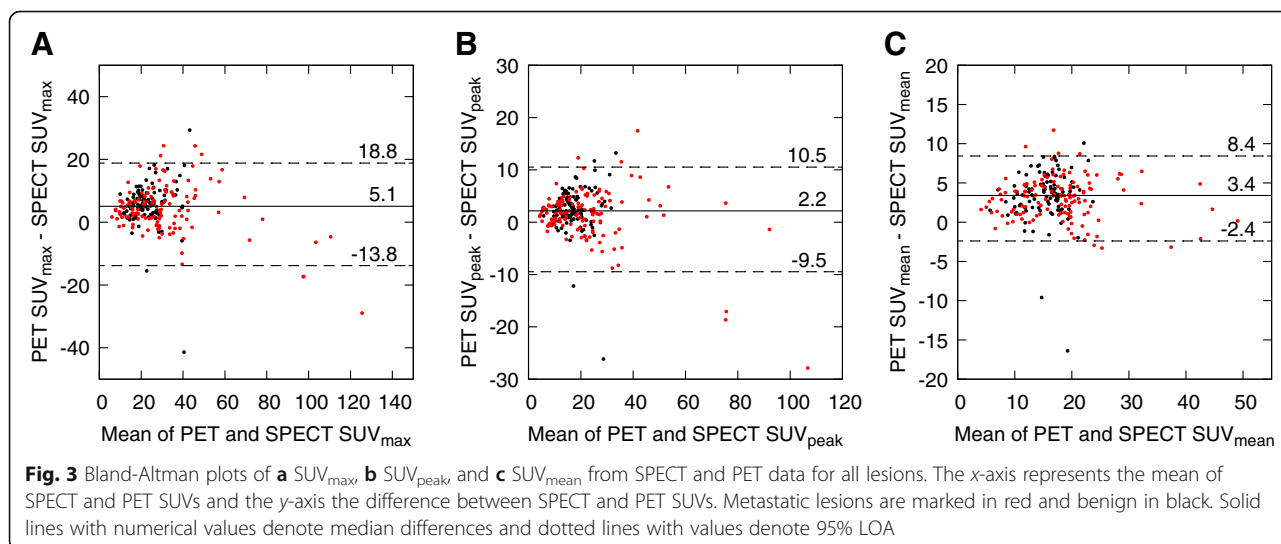


Table 2 Median (IQR) differences between SUVs of SPECT and PET for lesions in different size categories. The differences are normalized with respect to SPECT SUVs

Size category	n	SUV _{max}	SUV _{peak}	SUV _{mean}
0.55–1.21 cm ³	58	41% (–22–162%)	17% (–20–87%)	30% (–12–111%)
1.32–1.98 cm ³	58	24% (–24–89%)	11% (–39–52%)	19% (–34–63%)
1.98–3.97 cm ³	58	17% (–45–106%)	7% (–45–76%)	17% (–39–90%)
3.97–60.31 cm ³	57	11% (–29–83%)	6% (–26–52%)	17% (–14–51%)

In all our analyses, PET SUVs were systematically higher than SPECT SUVs. Due to poorer spatial resolution, underestimation of SUV caused by the partial volume effect is more significant in SPECT than PET [1]. However, a higher number of OSEM iterations in SPECT and wide Gaussian filters in PET were used to compensate for this resolution difference between SPECT and PET. This compensation roughly halved the absolute differences between the SUVs of SPECT and PET and reduced the differences in SUV_{R,max} and SUV_{R,mean} between SPECT and PET by 17 and 6 percentage units, respectively. The difference in SUV_{R,peak} increased by 6 percentage units.

After the compensation, the SUVs of PET were still significantly higher, even in background bone where no significant partial volume effect is expected. This suggests that a higher fraction of ¹⁸F-NaF than ^{99m}Tc-HDP is extracted from blood by bone. This difference is most likely caused by the different pharmacokinetics of ^{99m}Tc-HDP and ¹⁸F-NaF. For instance, blood protein binding hinders the extraction of ^{99m}Tc-diphosphonates but does not affect the ¹⁸F-NaF extraction [24–26]. The SUV differences were also larger in smaller lesions, which suggests that some difference was caused by the different spatial resolutions of SPECT and PET systems even after the compensation.

In this study, SUV_Rs were not significantly different between SPECT and PET. Previously, the SUV_R has been used mainly in the interpretation of brain PET. The SUV differences of lesions between different skeletal areas are partly caused by the differences in SUV_{S,mean,bg} between these areas, the highest SUVs and SUV_{S,mean,bg} being in the spine and the lowest in the skull. SUVs of lesions and their corresponding SUV_{S,mean,bg} cause that SUV_Rs are more similar than

corresponding SUVs between different skeletal sites, and being also very similar between SPECT and PET. The similarity of SUV_Rs between SPECT and PET arises the question whether SUV_Rs should be used instead of SUVs for the evaluation of metastatic uptake, both in quantitative PET and especially in quantitative SPECT. SUV_Rs can be calculated without scanner calibration or information on the patient weight or injected dose, making them technically easier to accomplish than SUVs and equal to target-to-background ratios. However, reliable calculation of SUV_{S,mean,bg} is manually laborious and sensitive to inter-observer variability; thus, the procedure should ideally be automatized.

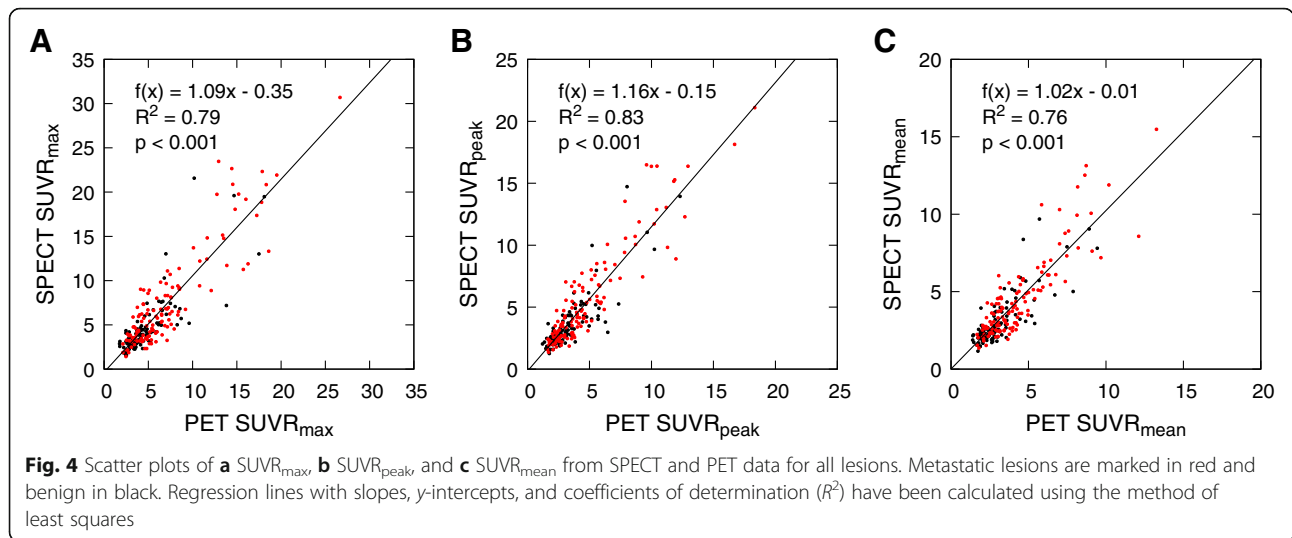
The typical SUV measure in PET has been SUV_{max} due to its simplicity and nonexistent inter-observer variability [27]. However, SUV_{max} is subject to noise and statistical variations in data [28]. Consequently, SUV_{peak} and SUV_{mean} have gained interest as robust alternatives to SUV_{max}. Also in this study, SUV_{peak} and SUV_{mean} were more similar than SUV_{max} between SPECT and PET. The strongest correlation and smallest systematic difference between SPECT and PET were in SUV_{peak}, which is measured as an average SUV of voxels in a 1-cm³ cube. Due to finite voxel size, the volumes of cubes were not exactly 1 cm³. In fact, the SUV_{peak} of SPECT was calculated from a 26% smaller volume than the SUV_{peak} of PET. This somewhat compensates for the generally higher SUVs of PET, which may partly result in the smallest difference in SUV_{peak}. The SPECT SUV_{peak} and SUV_{max} as well, may have also been slightly overestimated due to collimator response correction artifact [29]. These same factors increasing SPECT SUV_{peak} may also cause SPECT SUV_{R,peak} to be higher than PET SUV_{R,peak} resulting in the largest systematic difference among our SUV_R measures. However, the absolute differences we found between the SUV_Rs of SPECT and PET were generally very small.

Table 3 SUV_{S,mean,bg} from normal appearing bone at different skeletal sites

Skeletal site	PET SUV median (IQR)	SPECT SUV median (IQR)	PET SUV–SPECT SUV median (IQR)*
Skull	2.6 (2.1–5.0)	2.0 (1.8–2.6)	0.3 (0.1–0.8) (<i>p</i> < 0.01)
Spine	7.4 (6.6–8.7)	6.1 (4.7–6.8)	1.7 (0.6–2.8) (<i>p</i> < 0.001)
Rib cage	3.0 (2.4–4.0)	2.5 (2.0–3.1)	0.7 (–0.1–1.0) (<i>p</i> < 0.001)
Pelvis	5.5 (4.7–6.6)	4.7 (4.1–6.0)	0.6 (–0.2–1.3) (<i>p</i> < 0.01)
Limbs	3.8 (2.9–4.9)	3.2 (2.1–4.3)	0.7 (0.1–1.0) (<i>p</i> < 0.01)

IQR interquartile range

**p* value denotes at which level a median difference is significantly different from 0 according to the Wilcoxon signed rank test

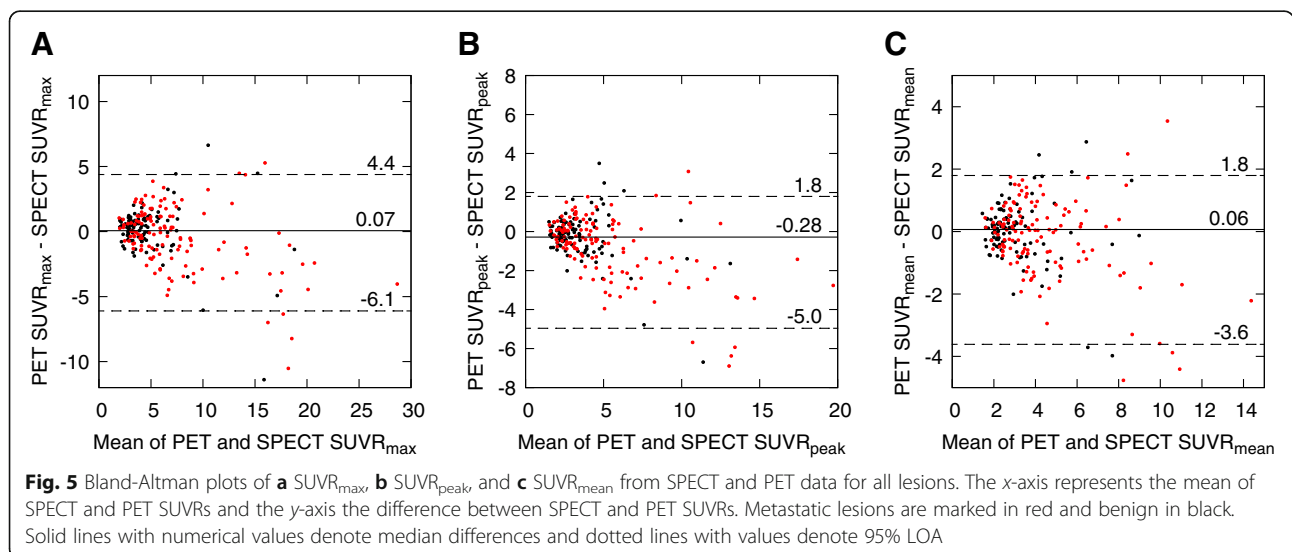


The strong correlation of SUVs and very similar SUVs between ^{99m}Tc -HDP SPECT and ^{18}F -NaF PET suggest that the SUVs and SUVRs of ^{99m}Tc -HDP SPECT are valid and feasible for research and clinical use. These results encourage SPECT SUVs to be utilized in clinical trials and follow-up studies to decrease inter-observer variability and to standardize SPECT results between patients, imaging systems, and clinical centers. Even though ^{18}F -NaF PET/CT is a more sensitive method than ^{99m}Tc -HDP SPECT/CT, the cost of ^{18}F -NaF PET/CT is three- to four-fold that of ^{99m}Tc -HDP SPECT/CT [6], making ^{99m}Tc -HDP SPECT/CT the more cost-effective modality for the evaluation of metastatic bone uptake in breast and prostate cancer. SPECT has also wider availability than PET in most countries [2]. The SUV regression lines have slopes so close to one that the SUVs of SPECT and PET would even be equal in some cases if a small positive bias

was added into SPECT SUV. However, because the Bland-Altman plots show rather wide 95% LOA, PET SUVs cannot be directly converted into SPECT SUVs. Therefore, usage of SPECT as follow-up for PET is not recommended.

The requirements for producing quantitative SPECT and PET data are the same. The most important ones are scanner calibration and a reconstruction algorithm correcting for photon attenuation and scatter within the object [1]. The calculation of reliable SUVs also requires accurate measurements of prepared activity, preparation time, injection time, syringe residual activity, time of residual activity measurement, and patient weight.

The main limitations of our study are the relatively small number of patients with bone metastases and the lack of accurate injected activities used in SPECT. We have afterwards measured the distribution of injected



activities from a sample of 38 syringes used for bone scans at our department. Our average injected activity should be 670 MBq. In that estimation, the injected activity was calculated as the activity of full syringe subtracted by the residual activity, and it had an average of 672 MBq and SD of 21 MBq. This average injected activity was eventually used in the SPECT SUV calculations of this study. We assume that the inaccuracy in the assessment of injected activity results in a maximum random error of 7% (= 2 SDs) in the individual SPECT SUV calculations and no error in the SPECT SUVR calculations. This error in SPECT SUV calculations is relatively small compared to SUV differences between SPECT and PET, so it does not have a significant influence on the statistical differences between SPECT and PET SUVs.

Conclusion

The SUVs of ^{99m}Tc -HDP SPECT/CT and ^{18}F -NaF PET/CT correlate strongly and SUVRs are very similar, showing that SPECT SUVs are feasible for uptake measurements in bone metastases of breast and prostate cancer. SUVs and SUVRs could be used to expand the visual analysis of skeletal SPECT especially in follow-up studies. The SUVs of ^{99m}Tc -HDP SPECT/CT are slightly lower than the SUVs of ^{18}F -NaF PET/CT.

Abbreviations

3D: Three-dimensional; CT: Computed tomography; DWI: Diffusion-weighted imaging; FWHM: Full width at half maximum; HDP: Hydroxyethylene diphosphonate; IQR: Interquartile range; LOA: Limits of agreement; MRI: Magnetic resonance imaging; OSEM: Ordered-subset expectation-maximization; PET: Positron emission tomography; PSA: Prostate-specific antigen; ROI: Region of interest; SD: Standard deviation; SPECT: Single-photon emission computed tomography; SUV: Standardized uptake value; SUVR: Standard uptake value ratio; VOI: Volume of interest

Acknowledgements

Radiographers and medical laboratory technologists at the Department of Nuclear Medicine and PET Centre of Turku University Hospital are acknowledged for patient preparation and image acquisition. Chris Constable at HERMES Medical Solutions AB is acknowledged for assistance in SPECT scanner calibration and image analyses.

Funding

This study was funded by Emil Aaltonen foundation, University of Turku and Turku University Hospital.

Availability of data and materials

The data supporting the findings of this study are included in this published article.

Authors' contributions

SA and TN designed the study. All authors participated in the data acquisition. SA and IJ analyzed the data. SA and TN drafted the manuscript. IJ, AK, JK, SK, and MS commented on the manuscript, and all authors approved the final version of the manuscript.

Ethics approval and consent to participate

This study was approved by the Ethics Committee of the Hospital District of Southwest Finland and each patient gave written informed consent.

Consent for publication

Each patient gave written informed consent for publication.

Competing interests

The authors declare that they have no competing interests.

Publisher's Note

Springer Nature remains neutral with regard to jurisdictional claims in published maps and institutional affiliations.

Author details

¹Department of Clinical Physiology and Nuclear Medicine, Turku University Hospital, Kiinamylynkatu 4-8, 20521 Turku, Finland. ²Department of Diagnostic Radiology, University of Turku, Turku, Finland. ³Department of Oncology and Radiotherapy, University of Turku, Turku, Finland. ⁴Turku PET Centre, Turku, Finland. ⁵Department of Medical Physics, Turku University Hospital, Turku, Finland.

Received: 29 November 2018 Accepted: 15 January 2019

Published online: 24 January 2019

References

- Bailey DL, Willows KP. An evidence-based review of quantitative SPECT imaging and potential clinical applications. *J Nucl Med.* 2013;54:83–9.
- Cachovan M, Vija AH, Hornegger J, Kuwert T. Quantification of ^{99m}Tc -DPD concentration in the lumbar spine with SPECT/CT. *EJNMMI Res.* 2013;3:1–8.
- Bailey DL, Willows KP. Quantitative SPECT/CT: SPECT joins PET as a quantitative imaging modality. *Eur J Nucl Med Mol Imaging.* 2014;41:S17–25.
- Ritt P, Vija H, Hornegger J, Kuwert T. Absolute quantification in SPECT. *Eur J Nucl Med Mol Imaging.* 2011;38(Suppl 1):S69–77.
- Hörger M, Bares R. The role of single-photon emission computed tomography/computed tomography in benign and malignant bone disease. *Semin Nucl Med.* 2006;36:286–94.
- Jambor I, Kuisma A, Ramadan S, Huovinen R, Sandell M, Kajander S, et al. Prospective evaluation of planar bone scintigraphy, SPECT, SPECT/CT, ^{18}F -NaF PET/CT and whole body 1.5T MRI, including DWI, for the detection of bone metastases in high risk breast and prostate cancer patients: SKELETA clinical trial. *Acta Oncol.* 2016;55:59–67.
- Römer W, Nömayr A, Uder M, Bautz W, Kuwert T. SPECT-guided CT for evaluating foci of increased bone metabolism classified as indeterminate on SPECT in cancer patients. *J Nucl Med.* 2006;47:1102–6.
- Even-Sapir E, Metser U, Mishani E, Lievshitz G, Lerman H, Leibovitch I. The detection of bone metastases in patients with high-risk prostate cancer: ^{99m}Tc -MDP planar bone scintigraphy, single- and multi-field-of-view SPECT, ^{18}F -fluoride PET, and ^{18}F -fluoride PET/CT. *J Nucl Med.* 2006;47:287–97.
- Sunderland JJ, Christian PE. Quantitative PET/CT scanner performance characterization based upon the society of nuclear medicine and molecular imaging clinical trials network oncology clinical simulator phantom. *J Nucl Med.* 2015;56:145–52.
- Brenner W, Vernon C, Muzi M, Mankoff DA, Link JM, Conrad EU, et al. Comparison of different quantitative approaches to ^{18}F -fluoride PET scans. *J Nucl Med.* 2004;45:1493–500.
- Beck M, Sanders JC, Ritt P, Reinfelder J, Kuwert T. Longitudinal analysis of bone metabolism using SPECT/CT and ^{99m}Tc -diphosphonopropanedicarboxylic acid: comparison of visual and quantitative analysis. *EJNMMI Res.* 2016;6:60–8.
- Suh MS, Lee WW, Kim Y-K, Yun P-Y, Kim SE. Maximum standardized uptake value of (^{99m}Tc) hydroxymethylene diphosphonate SPECT/CT for the evaluation of temporomandibular joint disorder. *Radiology.* 2016;280:890–6.
- Kaneta T, Ogawa M, Daisaki H, Nawata S, Yoshida K, Inoue T. SUV measurement of normal vertebrae using SPECT/CT with ^{99m}Tc methylene diphosphonate. *Am J Nucl Med Mol Imaging.* 2016;6:262–8.
- Kuji I, Yamane T, Seto A, Yasumizu Y, Shirotake S, Oyama M. Skeletal standardized uptake values obtained by quantitative SPECT/CT as an osteoblastic biomarker for the discrimination of active bone metastasis in prostate cancer. *Eur J Hybrid Imaging.* 2017;1:2–17.
- Messa C, Goodman WG, Hoh CK, Choi Y, Nissenson AR, Salusky IB, et al. Bone metabolic activity measured with positron emission tomography and ^{18}F -fluoride ion in renal osteodystrophy: correlation with bone histomorphometry. *J Clin Endocrinol Metab.* 1993;77:949–55.
- Piert M, Zittel TT, Becker GA, Jahn M, Stahlschmidt A, Maier G, et al. Assessment of porcine bone metabolism by dynamic ^{18}F -fluoride PET: correlation with bone histomorphometry. *J Nucl Med.* 2001;42:1091–100.

17. Lin C, Bradshaw T, Perk T, Harmon S, Eickhoff J, Jallow N, et al. Repeatability of quantitative ^{18}F -NaF PET: a multicenter study. *J Nucl Med*. 2016;57:1872–9.
18. Wassberg C, Lubberink M, Sörensen J, Johansson S. Repeatability of quantitative parameters of ^{18}F -fluoride PET/CT and biochemical tumour and specific bone remodelling markers in prostate cancer bone metastases. *EJNMMI Res*. 2017;7:42–9.
19. Hudson HM, Larkin RS. Accelerated image reconstruction using ordered subsets of projection data. *IEEE Trans Med Imaging*. 1994;13:601–9.
20. Sohlberg A, Watabe H, Iida H. Three-dimensional SPECT reconstruction with transmission-dependent scatter correction. *Ann Nucl Med*. 2008;22:549–56.
21. Sohlberg A, Watabe H, Iida H. Acceleration of Monte Carlo-based scatter compensation for cardiac SPECT. *Phys Med Biol*. 2008;53:N277–N85.
22. McCarthy AW, Miller M. Maximum likelihood SPECT in clinical computation times using mesh-connected parallel computers. *IEEE Trans Med Imaging*. 1991;10:426–36.
23. Boellaard R, O'Doherty MJ, Weber WA, Mottaghy FM, Lonsdale MN, Stroobants SG, et al. FDG PET and PET/CT: EANM procedure guidelines for tumour PET imaging: version 1.0. *Eur J Nucl Med Mol Imaging*. 2010;37:181–200.
24. Wong KK, Piert M. Dynamic bone imaging with $^{99\text{m}}\text{Tc}$ -labeled diphosphonates and ^{18}F -NaF: mechanisms and applications. *J Nucl Med*. 2013;54:590–9.
25. Segall G, Delbeke D, Stabin MG, Even-Sapir E, Fair J, Sajdak R, et al. SNM practice guideline for sodium ^{18}F -fluoride PET/CT bone scans 1.0. *J Nucl Med*. 2010;51:1813–20.
26. Grant FD, Fahey FH, Packard AB, Davis RT, Alavi A, Treves ST. Skeletal PET with ^{18}F -fluoride: applying new technology to an old tracer. *J Nucl Med*. 2007;49:68–78.
27. Wahl RL, Jacene H, Kasamon Y, Lodge MA. From RECIST to PERCIST: evolving considerations for PET response criteria in solid tumors. *J Nucl Med*. 2009;50:1225–50S.
28. Vanderhoek M, Perlman SB, Jeraj R. Impact of different standardized uptake value measures on PET-based quantification of treatment response. *J Nucl Med*. 2013;54:1188–94.
29. Kangasmaa T, Sohlberg A, Kuikka JT. Reduction of collimator correction artefacts with Bayesian reconstruction in Spect. *Int J Mol Imaging*. 2011; 2011:630813.

Submit your manuscript to a SpringerOpen[®] journal and benefit from:

- ▶ Convenient online submission
- ▶ Rigorous peer review
- ▶ Open access: articles freely available online
- ▶ High visibility within the field
- ▶ Retaining the copyright to your article

Submit your next manuscript at ▶ [springeropen.com](https://www.springeropen.com)